Radiology

Iterative Reconstruction Algorithm for Abdominal Multidetector CT at Different Tube Voltages: Assessment of Diagnostic Accuracy, Image Quality, and Radiation Dose in a Phantom Study[1]

Sebastian T. Schindera, MD
Lars Diedrichsen, MD
Hubert C. Müller, MD
Oliver Rusch, MD
Daniele Marin, MD
Bernhard Schmidt, PhD
Rainer Raupach, PhD
Peter Vock, MD
Zsolt Szucs-Farkas, MD

Purpose: To assess the diagnostic accuracy, image quality, and radiation dose of an iterative reconstruction algorithm compared with a filtered back projection (FBP) algorithm for abdominal computed tomography (CT) at different tube voltages.

Materials and Methods: A custom liver phantom with 45 simulated hypovascular liver tumors (diameters of 5, 10, and 15 mm; tumor-to-liver contrast of 10, 25, and 50 HU) was placed in a cylindrical water container that mimicked an intermediate-sized patient. The phantom was scanned at 120, 100, and 80 kVp. The CT data sets were reconstructed with FBP and iterative reconstruction. The image noise was measured, and the contrast-to-noise ratio (CNR) of the tumors was calculated. The radiation dose was assessed with the volume CT dose index. Tumor detection was independently performed by three radiologists. Statistical analysis included analysis of variance.

Results: Compared with the FBP data set at 120 kVp, the iterative reconstruction data set collected at 100 kVp demonstrated significantly lower mean image noise (20.9 and 16.7 HU, respectively; $P < .001$) and greater mean CNRs for the simulated tumors ($P < .001$). The iterative reconstruction data set collected at 120 kVp yielded the highest sensitivity for tumor detection, while the FBP data set at 80 kVp yielded the lowest. The sensitivity for the iterative reconstruction data set at 100 kVp was comparable with that for the FBP data set at 120 kVp (79.3% and 74.9%, respectively; $P > .99$). The volume CT dose index decreased by 39.8% between the 120-kVp protocol and the 100-kVp protocol and by 70.3% between the 120-kVp protocol and the 80-kVp protocol.

Conclusion: Results of this phantom study suggest that a 100-kVp abdominal CT protocol with an iterative reconstruction algorithm for simulated intermediate-sized patients increases the image quality and maintains the diagnostic accuracy at a reduced radiation dose when compared with a 120-kVp protocol with an FBP algorithm.

Supplemental material: *http://radiology.rsna.org/lookup/suppl/doi:10.1148/radiol.11102217/-/DC1*

[1] From the University Institute of Diagnostic, Interventional and Pediatric Radiology, University Hospital Bern, University of Bern, Freiburgstrasse 10, CH-3010 Bern, Switzerland (S.T.S., L.D., H.C.M., O.R., P.V., Z.S.); Department of Radiology, Duke University Medical Center, Durham, NC (D.M.); and Siemens Healthcare Sector, Forchheim, Germany (B.S., R.R.). Received November 16, 2010; revision requested January 11, 2011; final revision received February 15; accepted February 25; final version accepted March 3. **Address correspondence to** S.T.S. (e-mail: *sschindera@aol.com*).

In the past decade, the frequency of computed tomographic (CT) examinations increased substantially, mainly because of the technical advances and the wide availability of CT scanners. This development also resulted in an increase in exposure to ionizing radiation. Because ionizing radiation might be considered a carcinogen, when irradiating young to middle-aged patients in whom a sufficiently long latency period between exposure and effect can be anticipated, the number of radiation-induced cancers in the future will increase (1). Researchers in a recent publication estimated that approximately 29 000 new cancers every year in the United States could be related to past CT examinations (2). Half of these projected cancers were related to abdominal and pelvic CT examinations, which have the highest radiation doses among all types of CT scans (2). Because of this alarming assessment, the radiology community has been trying to find an optimized radiation exposure for patients undergoing CT examinations.

One of the approaches to lower the radiation dose is the application of lower tube voltage. A low-tube-voltage CT technique also provides improved contrast enhancement of iodine-containing vascular and parenchymal organs because it increases the x-ray absorption of iodine by decreasing the gap between the effective energy of the x-ray spectrum and the k edge of iodine (33.2 keV) (3). The disadvantage of lower tube voltage is greater image noise, particularly in abdominal and pelvic CT examinations. The increased image noise at lower tube voltages leads to a loss in image quality and a decrease in diagnostic accuracy. This concern about lower image quality prevented the clinical implementation of low-tube-voltage techniques in the past, particularly for abdominal CT applications in which the soft-tissue contrast is inherently lower.

Iterative reconstruction of image data, an imaging processing technique that was previously used in nuclear medicine, has been recently introduced for multidetector CT scanners with the goal of reducing image noise (4). In a recent clinical study on abdominal CT at 80 kVp, Marin and colleagues demonstrated improved image quality at a substantially lower radiation dose with adaptive statistical iterative reconstruction compared with the standard filtered back projection (FBP) (3). Other studies (4–7) on abdominal CT with use of a tube voltage of 120 kVp also showed the benefit of the adaptive statistical iterative reconstruction technique in terms of lower image noise and radiation dose. However, to our knowledge, the effect of an iterative reconstruction algorithm on low-contrast detectability in abdominal CT at different tube voltages has not been investigated. For such an assessment, a phantom study is an appropriate method because it does not require a separate reference standard and can be repeated multiple times with different CT parameters.

Thus, the objective of our liver phantom study was to assess the diagnostic accuracy, image quality, and radiation dose of the iterative reconstruction technique (Iterative Reconstruction in Image Space [IRIS]; Siemens Healthcare Sector, Forchheim, Germany) compared with the FBP technique for abdominal CT imaging at different tube voltages.

Advances in Knowledge

- In a phantom study, an iterative reconstruction algorithm (IRIS) improves the image quality and yields similar diagnostic accuracy in abdominal CT at the same tube voltage when compared with filtered back projection (FBP).
- At 120 kVp, the image noise decreased by 41.2% ($P < .001$), the contrast-to-noise ratio increased by 78.4% ($P < .001$), and the sensitivity for tumor detection was similar (74.9% for the FBP data set and 80.7% for the IRIS data set, $P > .99$) with the application of an IRIS algorithm in comparison with an FBP algorithm.
- Abdominal CT imaging at 100 kVp in combination with the IRIS algorithm for intermediate-sized patients yields a substantially lower radiation dose (39.8%) with comparable sensitivity (74.9% for FBP data set at 120 kVp and 79.3% for the IRIS data set at 100 kVp, $P > .99$) for tumor detection in comparison with a 120-kVp abdominal CT protocol with an FBP algorithm.

Implication for Patient Care

- The advantages of using the IRIS algorithm for a 100-kVp abdominal CT protocol include substantially reduced radiation dose, increased image quality, and a similar diagnostic accuracy in intermediated-sized patients compared with a standard 120-kVp abdominal CT protocol with an FBP algorithm.

Materials and Methods

Phantom

Siemens Healthcare Sector provided financial support for purchasing a custom liver phantom. Two authors (B.S. and R.R.) are employees of Siemens Healthcare Sector. However, the authors of this article who are not employees

Published online before print
10.1148/radiol.11102217 **Content codes:** GI PH

Radiology 2011; 260:454–462

Abbreviations:
CNR = contrast-to-noise ratio
FBP = filtered back projection
IRIS = Iterative Reconstruction in Image Space
ROI = region of interest

Author contributions:
Guarantors of integrity of entire study, S.T.S., H.C.M.; study concepts/study design or data acquisition or data analysis/interpretation, all authors; manuscript drafting or manuscript revision for important intellectual content, all authors; approval of final version of submitted manuscript, all authors; literature research, S.T.S., H.C.M.; clinical studies, L.D., H.C.M.; experimental studies, S.T.S., L.D., H.C.M., O.R., R.R.; statistical analysis, H.C.M., B.S., Z.S.; and manuscript editing, S.T.S., H.C.M., O.R., D.M., R.R., P.V., Z.S.

Potential conflicts of interest are listed at the end of this article.

of Siemens Healthcare Sector had complete control of any data and information that might present a conflict of interest to the authors who are employees.

The custom liver phantom (QRM, Moehrendorf, Germany) was manufactured to mimic the liver parenchyma at various tube voltages during the portal venous phase (Fig 1). To simulate hypovascular liver tumors, hypodense spherical lesions were embedded in the liver phantom. The material of the liver parenchyma and the tumors was composed of a homogeneous mixture of resin, including additives such as calcium carbonate and organic iodine. Thus, the attenuation of the simulated liver parenchyma and tumors represented the physical properties of attenuation in patients during the portal venous phase at different tube voltages. The custom attenuation specification of the liver and simulated tumors was obtained from a preliminary study in patients (Appendix E1 [online]).

The mean attenuation of the phantom liver parenchyma was measured to be 119.0 HU ± 4.7 [standard deviation] (range, 114–128 HU) at 120 kVp, 132.8 HU ± 5.7 (range, 129–146 HU) at 100 kVp, and 154.1 HU ± 3.2 (range, 149–161 HU) at 80 kVp. In total, 45 hypodense spherical lesions that simulated hypovascular liver tumors were embedded in the liver parenchyma. The tumors had three diameters (5, 10, and 15 mm) and three tumor-to-liver contrast values (10, 25, and 50 HU at 120 kVp). At 120 kVp, the mean attenuation of the tumor with a tumor-to-liver contrast of 10 HU measured 98.3 HU ± 2.5 (range, 95–102 HU), that for the tumor with a tumor-to-liver contrast of 25 HU measured 88.9 HU ± 6.6 (range, 81–99 HU), and that for the tumor with a tumor-to-liver contrast of 50 HU measured 74.1 HU ± 4.6 (range, 69–81 HU). Thus, for each size and tumor-to-liver contrast value combination, there were five simulated tumors. The distributions of the simulated tumors in the phantom were intentionally selected to achieve transverse CT images with multiple tumors, one tumor, or no tumors (Fig 2). The construction plan of the phantom served as the reference standard for this study. Although no lesion had a diameter of 5 mm and a tumor-to-liver contrast value of 10 HU in our preliminary study, we chose these specifications to simulate a worst-case scenario for lesion detection.

The spatial resolution was assessed in the x-y axes (transverse CT image) with the use of a high-contrast spatial-resolution phantom (QRM-3DSR; QRM) (Fig 3). The phantom consisted of a series of drilled holes with varying diameter and spacing from 4.0 mm down to 0.4 mm. The resulting line pairs per centimeter ranged between 1.25 and 12.5 line pairs per centimeter.

To simulate an intermediate-weight patient, the liver and spatial-resolution phantoms were placed in a water-filled cylindrical plastic container with a diameter of 30 cm (Figs 1, 3). The size of the container was selected to match the abdominal cross-sectional dimension of a patient with an estimated body weight ranging between 72 and 85 kg (8).

CT Scanning

The water container holding either the inserted liver phantom or the spatial-resolution phantom was scanned with a 64-section multidetector CT scanner (Somatom Sensation Cardiac 64; Siemens Healthcare Sector) with the use of tube-current–modulation software (CAREDose4D; Siemens Healthcare Sector). The phantom was scanned with three tube voltages (120, 100, and 80 kVp). All other CT parameters were kept the same in three protocols (160-mAs quality reference tube current–time product, gantry rotation speed of 0.5 second, 24 × 1.2-mm collimation, pitch of 1.15, and reconstructed section thickness of 1.5 and 5 mm). In addition to the standard FBP algorithm, all CT data sets were reconstructed with an IRIS algorithm. Thus, there were six CT data sets for the assessment of diagnostic accuracy and image quality.

The reconstruction algorithm of IRIS differs from the adaptive statistical iterative reconstruction technique, which has been extensively published (3–7,9). The IRIS approach is based on an initial master FBP reconstruction with a very sharp convolution kernel still containing all frequencies and therefore all information of the initial raw data (9). Subsequent iterative processing loops are applied to the image volume in which the image noise is reduced while sharpness is preserved, at the same time taking into account the physical properties of the scanner system and the reconstruction parameters. During each iteration, general image properties (eg, edge information and contrast-to-noise ratio [CNR]) are analyzed and used for the iterative reconstruction process. Therefore the iterative procedure enables a substantial noise reduction while preserving edge information and low-contrast structures.

When applying the IRIS algorithm, we used a reconstruction setting that was recommended by the CT manufacturer for abdominal CT examinations to achieve reasonable image noise reduction (approximately 40%) without affecting the overall appearance of the CT images. The setting offers a radiation dose reduction of at least 50% at a constant image quality.

Radiation Dose Assessment

For radiation dose assessment, the volume CT dose index was recorded for the scans at three tube voltages. The volume CT dose index was obtained from the dose page provided by the CT scanner.

Figure 1

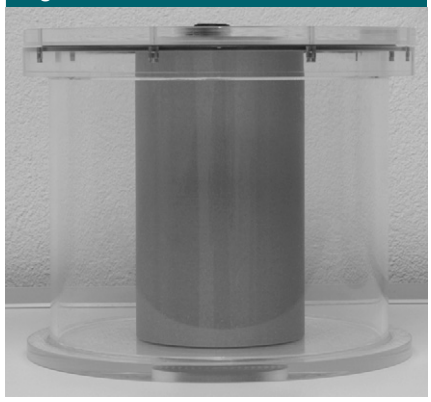

Figure 1: Image of the water container used to mimic an intermediate-sized patient. The container includes the cylindrical liver phantom (length, 25.5 cm; diameter, 15 cm) in its central axis.

Figure 2

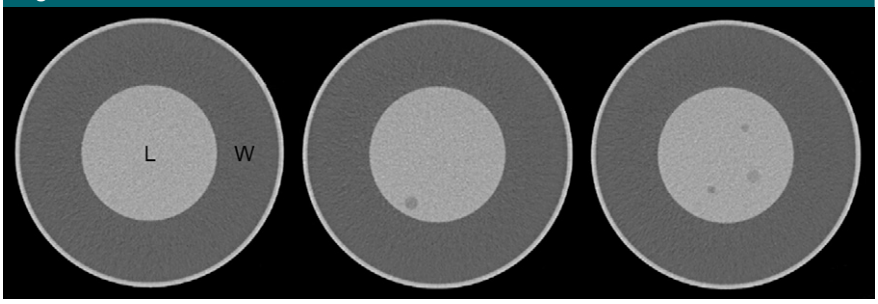

Figure 2: Three transverse CT images of the liver phantom *(L)* surrounded by water *(W)* acquired at three different levels. Left: CT image does not show any tumor. Middle: CT image demonstrates one 15-mm tumor with a tumor-to-liver contrast of 50 HU. Right: CT image shows two 10-mm tumors with a tumor-to-liver contrast of 50 HU and one 15-mm tumor with a tumor-to-liver contrast of 25 HU. The window width was 450 HU, and the window level was 50 HU for all images.

Figure 3

Figure 3: Image of the water container containing the spatial-resolution phantom in its central axis.

Assessment of Objective Image Quality and Spatial Resolution

Assessment of objective image quality was performed by the principal investigator (S.T.S., a radiologist with 7 years of experience in abdominal CT). The analysis was performed on 5-mm-thick transverse CT images on a high-definition liquid crystal display monitor (ME355i2; Totoku Electric, Tokyo, Japan) that had a display area of 423.9 × 318.0 mm, a maximum luminance of 1000 candela/m^2, and a maximum resolution of 2048 × 1536 pixels. The viewing distance was adjusted to the individual preference. CT attenuation values of the liver parenchyma and the tumors were obtained for the six CT data sets by manually placing circular regions of interest (ROIs). The size of the ROIs was measured to be on average 83 mm^2 (range, 70–96 mm^2) for the tumors and 977 mm^2 (range, 820–1180 mm^2) for the liver parenchyma. To avoid inaccuracies in a single measurement and misregistration due to small tumor size, three tumors with a 15-mm diameter and a tumor-to-liver contrast of 50 HU were used for attenuation measurements. The attenuation value of the liver parenchyma was measured adjacent to the tumors. To ensure consistency, all measurements were performed three times, and mean values were calculated. Image noise was defined as the standard deviation of the attenuation value measured in the liver parenchyma. The tumor-to-liver CNR was calculated as $CNR = (ROI_L - ROI_T)/N$, where ROI_L is the mean attenuation value of the liver parenchyma, ROI_T is the mean attenuation value of the simulated tumor, and N is noise.

For the assessment of spatial resolution, the 1.5-mm-thick transverse CT images were used. Two authors (Z.S. and S.T.S., with 14 and 7 years of experience in abdominal imaging, respectively) graded the spatial frequency in line pairs per centimeter in consensus.

Assessment of Lesion Detection and Subjective Image Quality

The 5-mm-thick transverse CT images were used for assessing lesion detection and image quality. Three radiologists (L.D., H.C.M., and O.R.), who had 5-6 years of experience in abdominal CT imaging, evaluated the six CT data sets independently on the same high-definition liquid crystal display monitor as was used in the assessment of image quality and spatial resolution. The readers were blinded to the number, location, and size of the simulated tumors, as well as to the scanning protocol. Before starting the assessment, each reader was given the criteria for image grading, and five test cases were together assessed. The readers were asked to mark the location of the tumors on evaluation sheets, along with the grade of conspicuity (grade 1, very poor, almost not visible; grade 2, poor; grade 3, intermediate; grade 4, good; grade 5, excellent). The readers first localized the tumor and then ranked the conspicuity. They also rated image noise (grade 1, major, unacceptable; grade 2, substantial, above average; grade 3, moderate, average; grade 4, minor, below average; grade 5, absent) and overall image quality (grade 1, bad, no diagnosis possible; grade 2, poor, diagnostic confidence substantially reduced; grade 3, moderate, but sufficient for diagnosis; grade 4, good; grade 5, excellent) for the entire CT data set. The six CT data sets were reviewed in six separate reading sessions in the following order: *(a)* FBP data set at 80 kVp, *(b)* FBP data set at 100 kVp, *(c)* FBP data set at 120 kVp, *(d)* IRIS data set at 80 kVp, *(e)* IRIS data set at 100 kVp, and *(f)* IRIS data set at 120 kVp. The reading sessions were separated by a minimum of 1 week. To minimize recall bias, the second and sixth CT data sets were rotated by 90°, the third CT data set was rotated by 180°, and the fourth CT data set was rotated by 270°, compared with the first CT data set. Although images were initially presented with a preset soft-tissue window (window width, 450 HU; window level, 50 HU), readers were allowed to modify the window width and level at their own discretion.

Statistical Analysis

The readers' marks on the evaluation sheets were compared with the real localization of the simulated tumors in the phantom. The reading sessions did not involve single CT images, and reviewers

Table 1

Descriptive Statistics for Various Tube Voltages and Image Reconstruction Algorithms

	120-kVp Protocol		100-kVp Protocol		80-kVp Protocol	
Parameter	FBP	IRIS	FBP	IRIS	FBP	IRIS
Image noise (HU)	20.9 ± 2.3	12.3 ± 1.4	28.5 ± 2.3	16.7 ± 1.6	46.9 ± 4.9	27.3 ± 3.0
Attenuation difference between tumor and liver (HU)*	46.0 ± 2.3	47.3 ± 1.5	57.6 ± 2.9	59.0 ± 2.3	75.2 ± 4.2	76.6 ± 2.3
CNR*	2.08 ± 0.28	3.71 ± 0.46	1.99 ± 0.19	3.48 ± 0.35	1.67 ± 0.19	2.81 ± 0.38

Note.—Values are means ± standard deviations. The volume CT dose index was 9.35 mGy for the 120-kVp protocol, 5.63 mGy for the 100-kVp protocol, and 2.78 mGy for the 80-kVp protocol.

* The data for the attenuation difference between tumor and liver and CNR were obtained for tumors with a diameter of 15 mm and a tumor-to-liver contrast of 50 HU at 120 kVp.

analyzed entire CT series with multiple simulated tumors. Thus, true-positive and false-positive findings and image quality parameters at various phantom settings were compared through analysis of variance for repeated measurements with post hoc tests and Friedman analysis of variance. Furthermore, multivariate analysis was performed with the use of tube voltage (80, 100, or 120 kVp) and image reconstruction algorithm (FBP or IRIS) as dependent variables. To rule out any possible influence of clustering effects, the probability of detecting a lesion was analyzed with respect to the number of lesions in the same image section. Interobserver agreement was assessed by calculating the weighted κ value. Agreement between the readers was graded as follows: poor, less than 0.20; fair, 0.21–0.40; moderate, 0.41–0.60; good, 0.61–0.80; and very good, 0.81–1.00 (10). A power analysis (at a power of 0.8 and α level of .05) was performed to determine the difference in sensitivity for the detection of the 45 lesions per tube voltage to identify significant differences between the FBP and IRIS algorithms. Statistical tests were performed with the use of software (StatSoft, Tulsa, Okla; MedCalc, MedCalc, Mariakerke, Belgium). *P* values of less than .05 were considered to indicate a significant difference.

Results

Radiation Dose

The radiation dose decreased by 39.8% between the 120-kVp and the 100-kVp protocols and by 70.3% between the 120-kVp and the 80-kVp protocols (Table 1).

Objective Image Quality and Spatial Resolution

The mean image noise decreased by approximately 41% at the three tube voltages for the IRIS algorithm when compared with the FBP algorithm ($P < .001$) (Table 1). The IRIS data set at 100 kVp demonstrated significantly lower mean image noise than did the FBP data set at 120 kVp (16.7 HU and 20.9 HU, respectively; $P < .001$). However, the mean image noise of the IRIS data set at 80 kVp was significantly greater than that of the FBP data set at 120 kVp (27.3 HU and 20.9 HU, respectively; $P < .001$).

The attenuation difference increased from 24.7% to 25.0% between 120 kVp and 100 kVp and from 62.0% to 63.5% between 120 kVp and 80 kVp ($P < .001$) (Table 1).

The mean CNRs for the tumors increased from 68.3% to 78.4% with the use of IRIS algorithm compared with the use of the FBP algorithm at the three tube voltages ($P < .001$) (Table 1). The IRIS data sets at 100 kVp yielded significantly higher mean CNRs than did the FBP data sets at 120 kVp ($P < .001$). In addition, the mean CNRs were significantly greater for the IRIS data sets at 80 kVp than for the FBP data sets at 120 kVp ($P < .001$).

The same spatial resolution was obtained in the FBP and IRIS data sets at 120 and 100 kVp (5.55 line pairs per centimeter). At 80 kVp, the spatial resolution decreased in the FBP and IRIS data sets (5.0 line pairs per centimeter).

Lesion Detection and Subjective Image Quality

The probability of detecting a lesion did not correlate with the number of simulated lesions in the same scan position, indicating that clustering effects might not have influenced our results ($P = .16$). The preliminary power analysis showed that our phantom with 45 lesions per tube voltage could confirm a difference of 8.3% in the sensitivity between FBP and IRIS at a power of 0.8 and α level of .05.

The overall detection of hypovascular tumors tended to be higher with the IRIS algorithm than with the FBP algorithm at all three tube voltages ($P > .05$) (Table 2). The IRIS data set at 120 kVp yielded the highest overall sensitivity, while the FBP data set at 80 kVp yielded the lowest overall sensitivity (Fig 4). The overall sensitivity of the IRIS data set at 100 kVp was similar to that of the FBP data set at 120 kVp (79.3% and 74.9%, respectively; $P > .99$). The data for detection of hypovascular tumors according to each reader are presented in Table 3.

The application of the IRIS algorithm yielded a significant difference for the overall true-positive rate for tumors with a diameter of 5 mm and a tumor-to-liver contrast of 50 HU ($P = .048$ and $P = .046$, respectively) (Table 4). The interobserver agreement among the three readers for the true-positive findings was good (mean weighted κ, 0.743; range, 0.672–0.881).

Neither the tube voltage (P = .2) nor the application of the IRIS algorithm (P = .4) had a significant effect on the grading of the overall conspicuity of the simulated hypovascular tumors (Table 2). The overall false-positive rate of the FBP data set at 120 kVp was significantly greater than that of the FBP data set at 100 kVp (P = .001) and 80 kVp (P = .01).

Overall image noise was rated by the three independent readers to be worse for the FBP data sets compared with the IRIS data sets at all three tube voltages (Table 5). Overall image noise was rated similarly for the IRIS data set at 100 kVp and the FBP data set at 120 kVp. The grading of the overall subjective image quality revealed that readers' rankings were lower for the FBP data sets than they were for the IRIS data sets at the same tube voltage (Table 5).

Table 2

Data for Detection of 45 Simulated Hypovascular Liver Tumors from Three Readers

Tube Voltage and Algorithm	Conspicuity*	No. of TP	No. of FP	No. of FN	Overall Sensitivity (%)
120 kVp					
FBP	2.38 (0.33, 4.67)	33.7	9	11.3	74.9
IRIS	2.48 (0.67, 4.67)	36.3	6.7	8.7	80.7
100 kVp					
FBP	2.45 (0.33, 4.67)	32.7	2	12.3	72.7
IRIS	2.46 (0.50, 4.83)	35.7	3.7	9.3	79.3
80 kVp					
FBP	2.22 (0.33, 4.33)	27.3	3.3	17.7	60.7
IRIS	2.52 (0.67, 4.67)	29.3	4.3	15.7	65.1

Note.—Data are means of results from three independent readers. FN = false-negative findings, FP = false-positive findings, TP = true-positive findings.

* The conspicuity of the tumors was rated on a five-point scale (grade 1 = very poor, almost not visible; grade 2 = poor; grade 3 = intermediate; grade 4 = good; and grade 5 = excellent). Data in parentheses are the 10th and 90th percentiles, respectively.

Figure 4

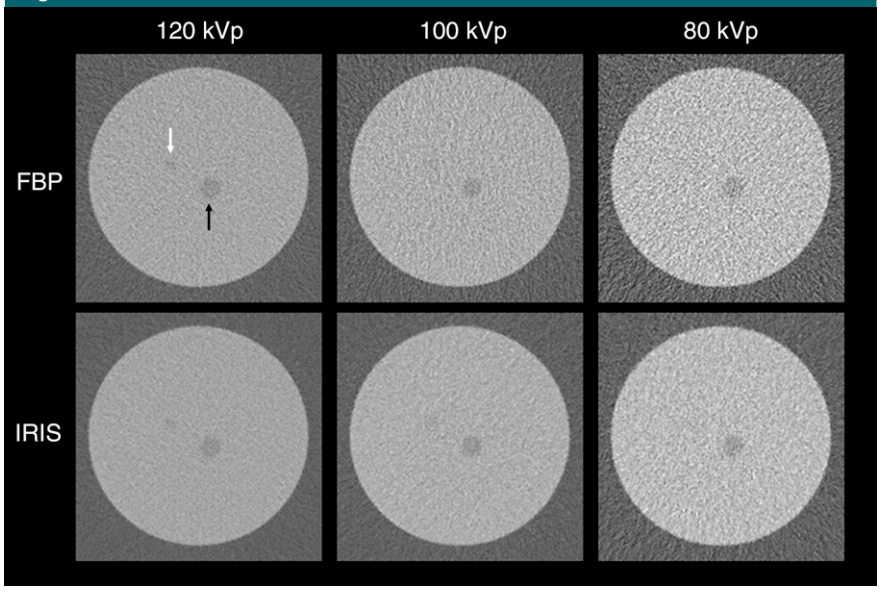

Figure 4: Cutouts of transverse CT images acquired at the same level of the liver phantom with three tube voltages. CT images were reconstructed either with the FBP or IRIS algorithm. At the presented level of the CT images, two liver tumors were simulated. Top left: Black arrow indicates a simulated 15-mm tumor with tumor-to-liver contrast of 25 HU and white arrow indicates a simulated 10-mm tumor with a tumor-to-liver contrast of 10 HU. On the 120-kVp data sets generated with the FBP and IRIS algorithms, the two simulated tumors were detected by all three readers. On the 100-kVp data sets generated with the FBP and IRIS algorithms, two readers detected the 10-mm tumor and three readers detected the 15-mm tumor. On the 80-kVp data sets generated with the FBP and IRIS algorithms, only the 15-mm tumor was detected by all three readers. The window width was 450 HU, and the window level was 50 HU for all images.

Discussion

Since the introduction of automatic tube-current modulation more than a decade ago, the iterative reconstruction algorithm has presented one of the most promising innovations for radiation dose reduction in abdominal CT. The first publications on adaptive statistical iterative reconstruction algorithms for abdominal CT demonstrated potential dose reduction up to 65% without any loss in image quality (3–6). The main shortcoming of those studies was that the diagnostic accuracy was not assessed. Currently, only the technical performance, which is the first level of six used for health technology assessment of diagnostic tools, has been evaluated (11). Thus, it is not known whether the reduced dose allowed by the iterative reconstruction algorithm for abdominal CT can lead to a reduction, preservation, or even enhancement of the diagnostic capability.

Our phantom study, which simulated an intermediated-sized patient, demonstrated similar overall sensitivity for detection of hypovascular liver tumors at a substantially lower radiation dose with the application of an IRIS algorithm. The radiation dose was reduced by almost 40% as the tube voltage decreased from 120 to 100 kVp, and the overall sensitivity was maintained when the IRIS data set at 100 kVp was compared with the FBP data set at 120 kVp. The spatial resolution was the same at 120 and 100 kVp in the FBP and IRIS data sets. But, how is it possible that

Table 3

Data for Detection of 45 Simulated Hypovascular Liver Tumors for Each Reader

Reader, Tube Voltage, and Algorithm	Conspicuity*	No. of TP	No. of FP	No. of FN
Reader 1				
120 kVp				
FBP	3.03 (1.0, 5.0)	33	5	12
IRIS	2.94 (1.0, 5.0)	34	1	11
100 kVp				
FBP	3.19 (1.0, 5.0)	31	0	14
IRIS	3.00 (1.0, 5.0)	33	1	12
80 kVp				
FBP	2.85 (1.0, 5.0)	27	1	18
IRIS	3.44 (2.0, 5.0)	27	2	18
Reader 2				
120 kVp				
FBP	2.58 (1.0, 4.0)	31	4	14
IRIS	2.08 (1.0, 4.0)	37	5	8
100 kVp				
FBP	2.50 (1.0, 4.0)	32	4	13
IRIS	2.47 (1.0, 4.7)	34	1	11
80 kVp				
FBP	2.58 (1.0, 4.0)	26	3	19
IRIS	2.25 (1.0, 4.0)	28	0	17
Reader 3				
120 kVp				
FBP	2.68 (1.0, 5.0)	37	18	8
IRIS	2.97 (1.0, 5.0)	38	12	7
100 kVp				
FBP	2.66 (1.0, 5.0)	35	2	10
IRIS	2.80 (1.0, 5.0)	40	10	5
80 kVp				
FBP	2.38 (1.0, 4.0)	29	6	16
IRIS	2.81 (1.0, 5.0)	33	9	12

Note.—Abbreviations are the same as for Table 2.

* Data are means. Numbers in parentheses are the 10th and 90th percentiles, respectively. Conspicuity was rated with the same five-point scale as specified in Table 2.

the IRIS algorithm can simultaneously achieve radiation dose reduction and maintain the diagnostic accuracy? There were probably two main factors that made this transformation possible. First, there was a substantial reduction in image noise with the utilization of the IRIS algorithm. The image noise in the IRIS data set at 100 kVp was significantly lower than that in the FBP data set at 120 kVp. Second, there was a greater attenuation difference between the hypovascular tumor and the hepatic parenchyma at lower tube voltages. This difference was because the hepatic parenchyma contained considerably more iodinated contrast medium than did the hypovascular tumor and the attenuation of the contrast material increased at lower x-ray tube voltages owing to greater photoelectric effect and decreased Compton scattering (12). A recent clinical investigation on dual-energy hepatic CT showed that the attenuation difference between hypovascular metastases and the liver parenchyma could be increased as the tube voltage decreased from 120 kVp to 80 kVp (13). The combination of the decreased image noise afforded by the IRIS algorithm and the augmented tumor-to-liver contrast owing to greater inherent attenuation of the iodinated contrast medium at lower tube voltages might result in similar diagnostic accuracy at a lower radiation dose for intermediate-sized patients undergoing abdominal CT at 100 kVp during the portal venous phase.

When low-tube-voltage abdominal CT scans are acquired during the portal venous phase, the increase of image noise has to be controlled because excessively high noise values can substantially diminish the detectability benefit of the increased tumor-to-liver contrast. The increased image noise at lower tube voltages can be controlled by increasing the tube current–time product and/or with the IRIS algorithm. In our study, image noise substantially increased and the detectability decreased at 80 kVp in spite of the use of the IRIS algorithm, because we used the same quality reference setting for the automatic tube-current modulation at all three tube voltages. This resulted in a substantial radiation dose reduction at the lower tube voltage but also resulted in substantially decreased sensitivity and image quality. In the clinical routine, the quality reference tube current–time product would be raised at 80 kVp. We intentionally did not adapt the quality reference tube current–time product at 80 kVp because we wanted to avoid the variability of the tube current among the protocols at various tube voltages.

In our phantom study, the highest overall sensitivity and CNRs were achieved for the IRIS data sets at 120 kVp. The 120-kVp CT protocol in combination with the IRIS algorithm could present a feasible strategy to improve image quality and diagnostic sensitivity in obese patients without increasing radiation dose. In future clinical studies, researchers should investigate the diagnostic accuracy and radiation dose efficiency of the IRIS algorithm for obese patients undergoing an abdominal CT examination during the portal venous phase.

Several potential limitations of our study merit consideration. First, although we observed a trend toward improved overall sensitivity with the IRIS algorithm at all three tube voltages, a significant difference between the two reconstruction algorithms was not found, possibly because our investigation was a phantom study with a small number

Table 4

Overall Number of True-Positive Findings Grouped according to Diameter, Tumor-to-Liver Contrast Value, and Tube Voltage

	Diameter			Tumor-to-Liver Contrast Value			Tube Voltage		
Algorithm and Statistic	5 mm (n = 45)	10 mm (n = 45)	15 mm (n = 45)	10 HU (n = 45)	25 HU (n = 45)	50 HU (n = 45)	80 kVp (n = 45)	100 kVp (n = 45)	120 kVp (n = 45)
FBP	10.3	38.7	44.6	25.3	31.7	36.7	27.3	32.7	33.7
IRIS	15	41.3	45	28	32.7	40.7	29.3	35.7	36.3
P value	0.048	0.16	0.32	0.56	0.42	0.046	0.37	0.09	0.21

Note.—Data were derived from reports of three independent and blinded readers.

Table 5

Data for Subjective Image Noise and Image Quality Separated by Each Reader and Derived from Three Readers

Parameter, Tube Voltage, and Algorithm	Reader 1	Reader 2	Reader 3	Overall
Image noise				
120 kVp				
FBP	4	3	4	3.7
IRIS	5	4	5	4.7
100 kVp				
FBP	4	3	3	3.3
IRIS	4	3	4	3.7
80 kVp				
FBP	3	2	2	2.3
IRIS	4	2	3	3.0
Image quality				
120 kVp				
FBP	4	5	4	4.3
IRIS	5	5	5	5.0
100 kVp				
FBP	3	3	5	3.7
IRIS	4	4	4	4.0
80 kVp				
FBP	2	2	2	2.0
IRIS	4	2	3	3.0

Note.—Image noise was rated on a five-point scale (grade 1 = major, unacceptable; grade 2 = substantial, above average; grade 3 = moderate, average; grade 4 = minor, below average; and grade 5 = absent), as was image quality (grade 1 = bad, no diagnosis possible; grade 2 = poor, diagnostic confidence substantially reduced; grade 3 = moderate, but sufficient for diagnosis; grade 4 = good; and grade 5 = excellent).

of simulated tumors. A greater number of simulated tumors might have resulted in a significant difference and might have allowed detailed analyses of lesion detection at a specific tumor diameter and tube voltage. Second, our liver phantom was simplified to mimic the enhancement condition of the hepatic parenchyma and hypovascular liver tumors existing momentarily during the portal venous phase. Our liver phantom, however, did not model heterogeneous parenchymal enhancement or distorted hepatic anatomy. Because parenchymal inhomogeneity may influence diagnostic accuracy and CNRs, it is important to confirm the results of our phantom study in vivo. Third, only the IRIS method was evaluated in the current study. Because the technical approaches of iterative reconstruction differ among CT manufacturers, our reported results may not apply to the iterative reconstruction technique of other manufacturers. Fourth, the review of the entire CT data sets for assessment of lesion detection may present an evaluation bias. However, because the reading sessions were separated by at least 1 week and the data sets were rotated, the risk of a recall bias is small.

In conclusion, our phantom study data demonstrated the implementation of a 100-kVp CT protocol in combination with the IRIS algorithm for intermediated-sized patients undergoing routine abdominal CT during the portal venous phase. This CT protocol demonstrates a similar overall sensitivity for detection of hypovascular liver tumors at a substantially lower radiation dose compared with a 120-kVp protocol with an FBP algorithm.

Disclosures of Potential Conflicts of Interest: S.T.S. Financial activities related to the present article: institution received payment for writing and reviewing the manuscript and provision of writing assistance, medicines, equipment, or administrative support from Siemens Healthcare Sector, author received a research grant from Siemens Healthcare Sector. Financial activities not related to the present article: institution received payment for manuscript preparation from Siemens Healthcare Sector. Other relationships: none to disclose. **L.D.** No potential conflicts of interest to disclose. **H.M.** No potential conflicts of interest to disclose. **O.R.** No potential conflicts of interest to disclose. **D.M.** No potential conflicts of interest to disclose. **B.S.** Financial activities related to the present article: none to disclose. Financial activities not related to the present article: is an employee of Siemens Healthcare Sector. Other relationships: none to disclose. **R.R.** Financial activities related to the present article: is an employee of Siemens Healthcare Sector. Financial activities not related to the present article: is an employee of and owns stock or stock options from Siemens Healthcare Sector. Other relationships: none to disclose. **P.V.** No potential conflicts of interest to disclose. **Z.S.** No potential conflicts of interest to disclose.

References

1. Brenner DJ, Hall EJ. Computed tomography: an increasing source of radiation exposure. N Engl J Med 2007;357(22):2277–2284.
2. Berrington de González A, Mahesh M, Kim KP, et al. Projected cancer risks from computed tomographic scans performed in the United States in 2007. Arch Intern Med 2009;169(22):2071–2077.
3. Marin D, Nelson RC, Schindera ST, et al. Low-tube-voltage, high-tube-current multidetector abdominal CT: improved image quality and decreased radiation dose with adaptive statistical iterative reconstruction algorithm—initial clinical experience. Radiology 2010;254(1):145–153.
4. Hara AK, Paden RG, Silva AC, Kujak JL, Lawder HJ, Pavlicek W. Iterative reconstruction technique for reducing body radiation dose at CT: feasibility study. AJR Am J Roentgenol 2009;193(3):764–771.
5. Flicek KT, Hara AK, Silva AC, Wu Q, Peter MB, Johnson CD. Reducing the radiation dose for CT colonography using adaptive statistical iterative reconstruction: a pilot study. AJR Am J Roentgenol 2010;195(1):126–131.
6. Prakash P, Kalra MK, Kambadakone AK, et al. Reducing abdominal CT radiation dose with adaptive statistical iterative reconstruction technique. Invest Radiol 2010;45(4):202–210.
7. Singh S, Kalra MK, Hsieh J, et al. Abdominal CT: comparison of adaptive statistical iterative and filtered back projection reconstruction techniques. Radiology 2010;257(2):373–383.
8. Menke J. Comparison of different body size parameters for individual dose adaptation in body CT of adults. Radiology 2005;236(2):565–571.
9. Pontana F, Pagniez J, Flohr T, et al. Chest computed tomography using iterative reconstruction vs filtered back projection. I. Evaluation of image noise reduction in 32 patients. Eur Radiol 2011;21(3):627–635.
10. Landis JR, Koch GG. The measurement of observer agreement for categorical data. Biometrics 1977;33(1):159–174.
11. Sardanelli F, Hunink MG, Gilbert FJ, Di Leo G, Krestin GP. Evidence-based radiology: why and how? Eur Radiol 2010;20(1):1–15.
12. Schindera ST, Nelson RC, Mukundan S Jr, et al. Hypervascular liver tumors: low tube voltage, high tube current multi-detector row CT for enhanced detection—phantom study. Radiology 2008;246(1):125–132.
13. Robinson E, Babb J, Chandarana H, Macari M. Dual source dual energy MDCT: comparison of 80 kVp and weighted average 120 kVp data for conspicuity of hypo-vascular liver metastases. Invest Radiol 2010;45(7):413–418.